arXiv:hep-ph/9503320v1 14 Mar 1995

DTP/95/24
February 1995

The Measurement of M_W from the W^+W^- Threshold Cross Section at LEP2

W.J. Stirling

Departments of Physics and Mathematical Sciences, University of Durham
Durham DH1 3LE, England

Abstract

The rapid increase of the $e^+e^- \to W^+W^-$ cross section in the threshold region provides a method for measuring M_W at LEP2. The dependence of the theoretical cross section — including the effects of the finite W width, Coulomb interactions and initial state radiation — on the collider energy and on the mass and width of the W is investigated in order to deduce the optimal collider energy which maximizes the sensitivity to M_W. Statistical and systematic uncertainties are studied in detail. The background contribution from QCD four-jet production is estimated. It is shown that by running LEP2 at $\sqrt{s} \approx 161$ GeV and obtaining a luminosity of order 100 pb^{-1} per experiment, an uncertainty on the measured value of M_W of ± 70 MeV should be achievable.

1 Introduction

A precision measurement of the mass of the W boson is one of the most important physics goals of the LEP2 e^+e^- collider. The impact of such a measurement on tests of the Standard Model and constraints on new physics beyond is well documented, see for example Sec. 10 of Ref. [1] or Sec. 8 of Ref. [2].

The current 'world average' value is [3]

$$M_W = 80.23 \pm 0.18 \text{ GeV} , \tag{1}$$

obtained by combining the results from the three $p\bar{p}$ collider experiments: CDF, D0 and UA2. The precision will improve with increasing luminosity at the Tevatron collider. In fact it is likely that the error will decrease to $O(100)$ MeV in the next few years, and may ultimately be as small as 50 MeV [2]. Clearly the aim of LEP2 should be to at least match this level of precision.

At least three methods of measuring M_W at LEP2 have been proposed, see for example Refs. [1, 4]. The most direct method, and at first sight the most promising, is to reconstruct M_W directly from its hadronic decay products using the decay channels

$$W^+W^- \;\to\; q\bar{q}q\bar{q} , \tag{2}$$
$$W^+W^- \;\to\; q\bar{q}\ell\nu . \tag{3}$$

If, for example, an integrated luminosity of $\int \mathcal{L} \simeq 500$ pb^{-1} can be obtained at a collider energy in the range 170−200 GeV, then the statistical uncertainty for this method (combining four experiments) is well below 50 MeV [4]. Notwithstanding the difficulties of reconstructing and measuring hadronic jets, the systematic errors appear to be under control as well. There is, however, one important caveat. It has recently been argued [5] that 'colour reconnection' effects — strong interactions between the separate hadronic final states of each W in (2) — *may* distort the mass measurement. The studies which yield small systematic errors on M_W from reconstructing the four-jet final state assume that the W^+W^- system can be treated as a superposition of two separate W decays, an approximation which may not be valid at the necessary level of precision.

A second method of measuring M_W is to use the fact that the end-points of the lepton spectrum in $W^+W^- \to q\bar{q}\ell\nu$ depends quite sensitively on the W mass:

$$E_- \le E_\ell \le E_+ , \qquad E_\pm = \frac{\sqrt{s}}{4}\left(1 \pm \sqrt{1 - 4M_W^2/s}\right) . \tag{4}$$

The problem with this method is that the statistical error is large for the total luminosity envisaged at LEP2: the net branching ratio for the $q\bar{q}\ell\nu$ final state ($\approx 8/27$, for $\ell = e, \mu$) is quite small, and only a fraction of events close to the end-points are

sensitive to M_W. In Ref. [4] a statistical error on M_W of order 300 MeV was obtained using this method.

The third method, the subject of the present work, is to use the rapid increase of the W^+W^- cross section at $\sqrt{s} \sim 2M_W$ to measure the mass. Although the rise of the Born (on-shell W) cross section is quite sharp, $\sigma \sim \beta$ where $\beta^2 = 1 - 4M_W^2/s$, various effects, for example the finite W width, smear out the threshold cross section, and so in practice the procedure is to fit a theoretical expression for the cross section, with M_W a free parameter, to the data. The advantage of this method is that it is a direct 'kinematic' measurement of the W mass, in the sense that the dependence of the cross section on M_W near threshold comes mainly from the opening up of the phase space rather than from the matrix element. There are, however, several important questions to address: (i) is it necessary to run at several collider energes to scan the threshold region, or is it better to run at a single 'optimal' energy, (ii) what is the resulting statistical precision on the mass measurement, (iii) how accurately must the cross section be measured, and how precisely does the theoretical cross section have to be known, to keep the systematic uncertainties well below the statistical uncertainty?

In this paper we attempt to answer these questions. We first of all discuss in some detail the status of the theoretical calculation of the $e^+e^- \to W^+W^-$ cross section in the threshold region. We derive and use an expression which, we believe, contains the bulk of the higher-order effects. We then study the variation of this cross section with $\sqrt{s}$, M_W, Γ_W, ... to estimate the optimal collider energies, and the corresponding statistical and systematic uncertainties.

There have been several other recent studies along broadly similar lines. In the theoretical studies of Refs. [6, 7], the emphasis was on estimating the uncertainty on M_W as a function of the collider energy. More recently, ongoing studies within the LEP collaborations have also been reported [8, 9, 10]. These address additional issues such as the problem of background contributions to the cross section. Where these studies overlap with the present work, there is a large measure of agreement. Earlier work [11, 12, 13, 14, 15] focused mainly on theoretical issues concerning the calculation of the W^+W^- cross section at LEP2 energies, and also of the impact on the cross section of new physics beyond the Standard Model.

The present work is closest in spirit to Ref. [6], in which many of the concepts to be discussed below were first presented. However our study extends the analysis of Ref. [6] in several important ways. We include, for example, the leading Coulomb corrections which have a significant effect on the threshold cross section, and consequently on the extracted value of M_W. We also attempt to quantify the most important background cross section, and assess its contribution to the systematic uncertainty on the W mass.

2 Calculation of the W^+W^- cross section

It is not our intention to perform a complete calculation of the theoretical cross section including, for example, all next-to-leading order electroweak corrections or all background contributions. In fact the next-to-leading order electroweak corrections for four fermion (i.e. off-shell W^+W^-) production are only partially known at present, see for example Ref. [16] for a detailed and up-to-date review. Our aim instead is to use a theoretical cross section which includes the most important higher-order effects to quantify the dependence on M_W. We will then be able to estimate the effect on the extracted M_W value of subsequent small variations in the theoretical prediction.

We begin by writing the cross section, schematically,[1] as

$$\begin{aligned} \sigma &= \sigma_{\rm WW} + \sigma_{\rm bkd} \ , \\ \sigma_{\rm WW} &= \sigma_0^{\rm WW} \left(1 + \delta_{\rm EW} + \delta_{\rm QCD}\right) \ , \end{aligned} \tag{5}$$

where the various terms correspond to

(i) $\sigma_0^{\rm WW}$: the Born contribution from the 3 leading-order diagrams for $e^+e^- \to W^+W^-$ involving t-channel ν exchange and s-channel γ and Z exchange, calculated using off-shell W propagators.

(ii) $\delta_{\rm EW}$: higher-order electroweak radiative corrections, including loop corrections, real photon emission, etc.

(iii) $\delta_{\rm QCD}$: higher-order QCD corrections to W^+W^- final states containing $q\bar{q}$ pairs. Since we are only concerned with the *total* cross section in this study, the effect of these is to generate small corrections to the hadronic branching ratios which are entirely straightforward to calculate and take into account.

(iv) $\sigma_{\rm bkd}$: 'background' contributions, for example from non-resonant diagrams (e.g. $e^+e^- \to \mu^+\nu_\mu W^-$) and QCD contributions $e^+e^- \to q\bar{q}gg$, $q\bar{q}q\bar{q}$ to the four-jet final state.

We will begin by studying (i) and (ii) in detail to identify the dominant effects, and later estimate the size of the background contributions. Note that all the various theoretical components which we need for this study already exist in the literature.

[1] We note that this decomposition of the cross section into 'signal' and 'background' contributions is practical rather than theoretically rigorous, since neither contribution is separately gauge invariant nor experimentally distinguishable in general.

2.1 The W^+W^- off-shell cross section

The leading-order cross section for off-shell W^+W^- production was first presented in Ref. [17]:

$$\sigma(s) = \int_0^s ds_1 \int_0^{(\sqrt{s}-\sqrt{s_1})^2} ds_2 \; \rho(s_1)\rho(s_2) \; \sigma_0(s, s_1, s_2) \; , \tag{6}$$

where

$$\rho(s) = \frac{1}{\pi}\frac{\Gamma_W}{M_W} \; \frac{s}{(s - M_W^2)^2 + s^2\Gamma_W^2/M_W^2} \; . \tag{7}$$

Note that this expression uses a s-dependent W width,

$$\Gamma_W(s) = \frac{s}{M_W^2} \; \Gamma_W \; , \tag{8}$$

where $\Gamma_W \equiv \Gamma_W(M_W^2)$, as advocated in Ref. [6] for example. We will discuss this further below.

The cross section σ_0 can be written in terms of the ν, γ and Z exchange contributions and their interferences:

$$\sigma_0(s, s_1, s_2) = \frac{g^4}{256\pi s^2 s_1 s_2} \; \left[a_{\gamma\gamma} + a_{ZZ} + a_{\gamma Z} + a_{\nu\nu} + a_{\nu Z} + a_{\nu\gamma}\right] \; , \tag{9}$$

where $g^4 = e^4/\sin^4\theta_W$. For completeness, the expressions for the various contributions are listed in the Appendix. The stable (on-shell) W^+W^- cross section is simply

$$\sigma^{\rm on}(s) = \sigma_0(s, M_W^2, M_W^2) \; . \tag{10}$$

It will be an important factor in the discussion which follows that near threshold the cross section is completely dominated by the t-channel neutrino exchange diagram. This leads to an S-wave threshold behaviour $\sigma_t \sim \beta$, whereas the s-channel vector boson exchange diagrams give the characteristic P-wave behaviour $\sigma_s \sim \beta^3$.[2] This is illustrated in Fig. 1, which shows the on-shell cross section decomposed in terms of the six contributions of Eq. (9).

2.2 Higher-order electroweak corrections

The complete set of $O(\alpha)$ next-to-leading order corrections to W^+W^- production has been calculated by several groups, for the *on-shell* case only, see Ref. [16] and references therein. There has been some progress [18, 19] with the off-shell (i.e. four fermion production) corrections but the calculation is not yet complete. However using the on-shell calculations as a guide, it is already possible to predict some of the

[2] We only consider unpolarized e^+e^- collisions in this study.

largest effects. For example, it has been shown that close to threshold the dominant contribution comes from the Coulomb correction, i.e. the long-range electromagnetic interaction between almost stationary heavy particles. Also important is the emission of photons collinear with the initial state $e^{\pm}$ ('initial state radiation') which gives rise to logarithmic corrections $\sim \alpha \ln(s/m_e^2)$. These leading logarithms can be resummed to all orders, and incorporated for example using a 'structure function' formalism. In this case, the generalization from on-shell to off-shell W's appears to be straightforward. For the Coulomb corrections, however, one has to be much more careful, since in this case the inclusion of the finite W decay width has a dramatic effect. Finally, one can incorporate certain important higher-order fermion and boson loop corrections by a judicious choice of electroweak coupling constant. Each of these effects will be discussed in turn below.

In summary, certain $O(\alpha)$ corrections are already known to be large, because their coefficients involve large factors like $\log(s/m_e^2)$, $\sqrt{M_W/\Gamma_W}$, m_t^2/M_W^2, etc. Once these are taken into account, one may hope that the remaining corrections are no larger than $\alpha\times$ constant. When estimating the theoretical systematic uncertainty on the W mass in Section 5, we shall therefore assume an overall uncertainty on the cross section of $\pm 1\%$ from the as yet uncalculated $O(\alpha)$ corrections.

2.2.1 Coulomb corrections

This section is essentially a summary of the results of Refs. [20, 21], where the Coulomb corrections for on-shell and off-shell W^+W^- production have been discussed in detail, and where a complete set of references to earlier studies can be found.

The result for on-shell W^+W^- production is well known — the correction diverges as $1/v_0$ as the relative velocity v_0 of the W bosons approaches zero at threshold. Explicitly, to $O(\alpha)$,

$$\sigma_C(s) = \sigma_0(s)\,[1 + \delta_C(s)]\,, \tag{11}$$

where

$$\delta_C(s) = \frac{\alpha}{v_0}\,\pi\,, \tag{12}$$

with the relative velocity given by

$$v_0 = 2\sqrt{1 - \frac{4M_W^2}{s}}\,. \tag{13}$$

As the threshold is approached from above, $\delta_C \to \infty$ and the corrections must be resummed to all orders, giving [22]

$$1 + \frac{\alpha}{v_0} + \ldots \longrightarrow \frac{2\alpha\pi/v_0}{1 - \exp(-2\alpha\pi/v_0)}\,. \tag{14}$$

Note that $\sigma_0 \sim v_0$ near threshold and so the Coulomb-corrected cross section is formally non-vanishing when $\sqrt{s} = 2M_W$.

For unstable W^+W^- production the finite decay width Γ_W *screens* the Coulomb singularity [20], so that very close to threshold the perturbative expansion in α/v_0 is effectively replaced by an expansion in $\alpha\sqrt{M_W/\Gamma_W}$ [21]. The net effect is a correction which reaches a maximum of approximately +6% in the threshold region [23]. Although this does not appear to be large, we will see below that it changes the threshold cross section by an amount equivalent to a shift in M_W of order 100 MeV. The result for off-shell W^+W^- production is (cf. Eqs. (11,12))

$$\sigma(s) = \int_0^s ds_1 \int_0^{(\sqrt{s}-\sqrt{s_1})^2} ds_2 \; \rho(s_1)\rho(s_2) \; \sigma_0(s, s_1, s_2)[1 + \delta_C(s, s_1, s_2)] \tag{15}$$

where [21][3]

$$\delta_C(s, s_1, s_2) = \frac{\alpha}{v} \left[\pi - 2 \arctan\left(\frac{|\kappa|^2 - p^2}{2p \; \mathrm{Re}(\kappa)}\right)\right] \tag{16}$$

$$v = \frac{4p}{\sqrt{s}} = 2\sqrt{1 - \frac{(2s(s_1+s_2) - (s_1-s_2)^2)}{s^2}} \tag{17}$$

$$\kappa = \sqrt{-M_W(E + i\Gamma_W)}, \qquad E = \frac{s - 4M_W^2}{4M_W} \tag{18}$$

In Ref. [21] the above $O(\alpha)$ result is generalized to all orders. However the contributions from second order and above change the cross section by $\ll 1\%$ in the threshold region [24] and will be omitted in what follows.

2.2.2 Initial state radiation

Another important class of electroweak radiative corrections comes from the emission of photons from the incoming e^+ and e^-. In particular, the emission of virtual and soft real photons with energy $E < \omega$ gives rise to doubly logarithmic contributions $\sim \alpha \ln(s/m_e^2) \ln(s/\omega^2)$ at each order in perturbation theory. The infra-red ($\ln \omega$) logarithms cancel when hard photon contributions are added, and the remaining collinear ($\ln(s/m_e^2)$) logarithms can be resummed and incorporated in the cross section using a 'structure function' [25] (see also Refs. [26, 27, 28])

$$\sigma_{\mathrm{ISR}} = \int_{s_{\min}}^s \frac{ds'}{s} \; F(x, s)|_{x=1-s'/s} \; \sigma(s') \tag{19}$$

where [26]

$$F(x, s) = t x^{t-1} \; \mathcal{S} \; + \; \mathcal{H} \; , \tag{20}$$

[3]Note that in Ref. [23] a slightly different version of Eq. (16) is derived, but the numerical difference in the threshold region is very small. See Ref. [21] for a critical discussion.

$$\begin{aligned}
\mathcal{S} &= 1+\frac{3}{4}\,t \;+\; \left(\frac{9}{32}-\frac{\pi^2}{12}\right)\,t^2+\frac{\alpha}{\pi}\left(\frac{\pi^2}{3}-\frac{1}{2}\right)\;+\;\ldots \\
\mathcal{H} &= \left(\frac{x}{2}-1\right)\,t\;+\;\left[\left(\frac{x}{2}-1\right)\ln x-\frac{1+3(1-x)^2}{8x}\ln(1-x)+\frac{x}{8}-\frac{3}{4}\right]\,t^2\;+\;\ldots\,,
\end{aligned} \tag{21}$$

with

$$t=\frac{2\alpha}{\pi}\left[\ln\left(\frac{s}{m_e^2}\right)-1\right]\,. \tag{22}$$

The $\mathcal{S}$ term comes from soft and virtual photon emission, while the $\mathcal{H}$ term comes from hard collinear emission. Contributions up to $O(t^2)$ are included, as well as a finite soft-gluon contribution at $O(\alpha)$.

The incorporation of leading logarithmic effects in this way has been widely discussed in the literature, see for example Ref. [16] and references therein. In fact the form given above — in which the cross section is factorized into a structure function multiplying the Born cross section — is strictly only valid for processes where there is no transfer of electric charge between the initial and final state particles, e.g. $e^+e^-\to Z\to f\bar{f}$. Only the double logarithmic terms are in fact 'universal', i.e. process independent. In general, the subleading $O(\alpha)$ corrections do not factorize in the manner of Eq. (20). One possible refinement applicable to $e^+e^-\to W^+W^-$ involves the 'current splitting technique' of Ref. [29], in which a charge flow is artificially introduced into the t-channel neutrino exchange in order that a gauge invariant initial-state radiation contribution can be defined and factored out. In fact, close to the W^+W^- threshold the corrections obtained using the current splitting and universal ISR methods differ only at the 1% level [29]. This difference is in any case of the same order as the neglected final state radiation contributions.

2.2.3 Improved Born approximation

In the Standard Model, three parameters are sufficient to parametrize the electroweak interactions, and the conventional choice is $\{\alpha, G_\mu, M_Z\}$ since these are the three which are measured most accurately. In this case the value of M_W is a *prediction* of the model. Radiative corrections to the expression for M_W in terms of these parameters introduce non-trivial dependences on m_t and M_H, and so a measurement of M_W provides a constraint on these masses. However the choice $\{\alpha, G_\mu, M_Z\}$ does not appear to be well suited to W^+W^- production. The reason is that a variation of the parameter M_W, which appears explicitly in the phase space and in the matrix element, has to be accompanied by an adjustment of the charged and neutral weak couplings. Beyond leading order this is a complicated procedure.

It has been argued [30] that a more appropriate choice of parameters for LEP2 is the set $\{M_W, G_\mu, M_Z\}$ (the so-called G_μ–scheme), since in this case the quantity of

prime interest is one of the parameters of the model. Using the tree-level relation

$$g^2 = e^2/\sin^2\theta_W = 4\sqrt{2}G_\mu M_W^2 \tag{23}$$

we see that the dominant t-channel neutrino exchange amplitude, and hence the corresponding contribution to the cross section, depends only on the parameters M_W and G_μ. It has also been shown [30] that in the G_μ–scheme there are no large next-to-leading order contributions to the cross section which depend on m_t, either quadratically or logarithmically. One can go further and choose the couplings which appear in the other terms in the Born cross section such that all large corrections at next-to-leading order are absorbed, see for example Ref. [31]. However in this study we are only interested in the threshold cross section, and so we will simply use combinations of e^2 and g^2 defined by Eq. (23) for the neutral and charged weak couplings which appear in the Born cross section, Eq. (9).

In summary, the most model-independent approach when defining the parameters for computing the $e^+e^- \to W^+W^-$ cross section appears to be the G_μ–scheme, in which M_W appears explicitly as a parameter of the model. Although this makes a non-negligible difference when calculating the Born cross section, compared to using α and $\sin^2\theta_W$ to define the weak couplings (see Table 2 below), a full next-to-leading-order calculation will remove much of this scheme dependence [30].

parameter	value
M_Z	91.1888
M_W	80.23
Γ_Z	2.4974
Γ_W	2.078
α^{-1}	137.0359895
G_μ	1.16639×10^{-5} GeV^{-2}
$\sin^2\theta_W \equiv \sin^2\theta_W^{(\ell)\text{eff}}$	0.2320
m_e	5.1099906×10^{-4}
$(\hbar c)^2$	3.8937966×10^8 pb GeV^2

Table 1: Parameter values used in the numerical calculations. Masses and widths are given in GeV.

2.3 Numerical evaluation of the cross section

Figure 2 shows the $e^+e^- \to W^+W^-$ cross section at LEP2 energies. The different curves correspond to the sequential inclusion of the different effects discussed in the previous section. The parameters used in the calculation are listed in Table 1. Note that both the initial state radiation and the finite width smear the sharp threshold behaviour at $\sqrt{s} = 2M_W$ of the on-shell cross section. The different contributions are quantified in Table 2, which gives the values of the cross section in different approximations just above threshold ($\sqrt{s} = 161$ GeV) and at the standard LEP2 energy of $\sqrt{s} = 175$ GeV. At threshold we see that the effects of the intitial state radiation and the finite width are large and comparable in magnitude.

σ_{WW}	$\sqrt{s} = 161$ GeV	$\sqrt{s} = 175$ GeV
σ_0 (on-shell, α)	3.813	15.092
σ_0 (on-shell, G_μ)	4.402	17.425
σ_0 (off-shell with $\Gamma_W(M_W^2)$, G_μ)	4.747	15.873
σ_0 (off-shell with $\Gamma_W(s)$, G_μ)	4.823	15.882
$\ldots$ + $O(\alpha)$ Coulomb	5.122	16.311
$\ldots$ + $O(\alpha)$ Coulomb + ISR	3.666	13.620

Table 2: Decomposition of the theoretical $e^+e^- \to W^+W^-$ cross section (in picobarns) as defined and discussed in the text, at two LEP2 collider energies.

Our primary aim is to investigate the dependence of the cross section on M_W. We do this by taking the solid curve in Fig. 2 (G_μ, finite width, initial state radiation, Coulomb correction) as our 'baseline' prediction. Figure 3 shows the cross sections for $M_W = 80.0$ and 80.4 GeV, normalized to that for $M_W = 80.2$ GeV, as a function of the e^+e^- collider energy $\sqrt{s}$. As expected, the sensitivity to M_W is greatest near threshold. Note that for the on-shell cross section, with no initial state radiation, the lower curve would decrease to 0 at $\sqrt{s} = 160.8$ GeV and the upper curve would increase to ∞ at $\sqrt{s} = 160.4$ GeV. Figure 3 also shows the statistical uncertainty on the cross section ($\sim 1/\sqrt{N_{\rm ev}}$) which would be expected for $\int \mathcal{L} = 100$ pb^{-1} at each of four separate collider energies. The fact that this uncertainty increases as $\sqrt{s}$ decreases is simply a reflection of the decreasing cross section. However, it is immediately evident that the threshold region offers the highest statistical sensitivity to M_W. The point of optimal sensitivity will be discussed in the following section.

3 Sensitivity of the cross section to M_W

In this section we investigate which LEP2 collider energy offers the maximum precision on M_W from a cross-section measurement. There are several factors to take into consideration. The first concerns the statistical uncertainty. Far above threshold the number of W^+W^- events is large but this is outweighed by the very weak M_W dependence. Far below the (nominal) threshold there are too few events to achieve any precision. The second concerns the systematic uncertainties. The important non-W^+W^- background processes do not have the threshold energy dependence of the signal, and therefore constitute an increasingly large fraction of the event sample as the threshold energy is approached from above. The optimal collider energy must therefore take all these competing factors into account.

3.1 Statistical uncertainty

If $\int \mathcal{L}$ is available for measuring the cross section with an efficiency ϵ at a collision energy $\sqrt{s}$, then the statistical error on M_W can be estimated as

$$\Delta M_{\rm stat} = \left|\frac{d\sigma}{dM}\right|^{-1} \Delta\sigma = \left|\frac{d\sigma}{dM}\right|^{-1} \sqrt{\frac{\sigma}{\epsilon \cdot \int \mathcal{L}}} \equiv K \left[\epsilon \cdot \int \mathcal{L}\right]^{-\frac{1}{2}} , \tag{24}$$

where

$$K = \sqrt{\sigma} \left|\frac{d\sigma}{dM}\right|^{-1} \tag{25}$$

is a measure of the sensitivity to M_W. The dependence of K on $\sqrt{s}$ is shown in Fig. 5. There is evidently a fairly sharp minimum just ($\sim$ 500 MeV) above the nominal threshold of $\sqrt{s} = 2M_W$, at which point

$$\Delta M_{\rm stat} \;=\; 90 \text{ MeV} \; \left[\frac{\epsilon \cdot \int \mathcal{L}}{100 \text{ pb}^{-1}}\right]^{-\frac{1}{2}} . \tag{26}$$

3.2 Systematic uncertainties

If the cross section is subject to an overall *multiplicative* factor C with an uncertainty ΔC (high-order corrections, luminosity, efficiency, ...) then the associated systematic error is

$$\Delta M_{\rm sys} \;=\; \left|\frac{d\sigma}{dM}\right|^{-1} \sigma \, \frac{\Delta C}{C} \;\equiv\; J \, \frac{\Delta C}{C} , \tag{27}$$

where

$$J = \sigma \left|\frac{d\sigma}{dM}\right|^{-1} . \tag{28}$$

The quantity J is shown in Fig. 6 as a function of $\sqrt{s}$. Again we see that the curve has a minimum in the threshold region. At the energy ($\sqrt{s} \simeq 161$ GeV) at which K is minimized we see that $J \simeq 1.7$ GeV, and so

$$\Delta M_{\rm sys} \;\simeq\; 17 \text{ MeV} \;\left[\frac{\Delta C}{C} \times 100\%\right] \;. \tag{29}$$

For an *additive* uncertainty (for example from the subtraction of a non-WW background cross section, see below) the contribution to the systematic error is simply

$$\Delta M_{\rm sys} \;=\; \left|\frac{d\sigma}{dM}\right|^{-1} \;\Delta\sigma \;\equiv\; L\,\Delta\sigma \;. \tag{30}$$

The quantity L is shown in Fig. 7 as a function of $\sqrt{s}$ in the threshold region. The curve has a similar shape to the statistical sensitivity function shown in Fig. 5, although the minimum is not quite as sharp. At the energy ($\sqrt{s} \simeq 161$ GeV) at which K is minimized we see that

$$\Delta M_{\rm sys} \;=\; 470 \text{ MeV} \;\left[\frac{\Delta\sigma}{1 \text{ pb}}\right] \;. \tag{31}$$

Finally, there is in principle a systematic uncertainty in M_W arising from an uncertainty in the beam energy. It is already apparent from Fig. 4 that a shift in the beam energy is equivalent to a shift in M_W. Quantitatively,

$$\Delta M_{\rm sys} \;=\; \left|\frac{d\sigma/dE_{\rm beam}}{d\sigma/dM}\right| \;\Delta E_{\rm beam} \;. \tag{32}$$

The ratio of derivatives is almost independent of energy in the threshold region and has a numerical value very close to 1, i.e.

$$\Delta M_{\rm sys} \;\simeq\; 1.0 \;\Delta E_{\rm beam} \;. \tag{33}$$

Current estimates suggest that a $\Delta E_{\rm beam}$ of less than 15 MeV can be achieved [32], and so the systematic error from this source is not expected to be particularly significant.

3.3 Dependence of the cross section on Γ_W

In the Standard Model, the decay width of the W is

$$\begin{aligned} \Gamma_W \;&=\; [3 + 6\{1 + \alpha_s(M_W)/\pi + ...\}]\;\Gamma(W \to \ell\nu) \\ &=\; [0.1084 \pm 0.0002]\;\frac{G_\mu M_W^3}{\sqrt{2}\,6\pi}\;\left(1 + \delta^{\rm SM}\right) \;, \end{aligned} \tag{34}$$

where $\alpha_s(M_W) = 0.12 \pm 0.01$ is used in the leptonic branching ratio. The higher order electroweak corrections depend weakly on m_t and M_H, and for canonical values of

these $\delta^{\rm SM} = -0.0035$ [35, 36] (see also [37]). The main uncertainty therefore comes from the value of M_W itself,

$$\Gamma_W = 2.078 \left(\frac{M_W}{80.23 \text{ GeV}}\right)^3 \text{ GeV} . \tag{35}$$

If we use the current world average value (Eq. (1)) for M_W then $\Gamma_W = 2.078 \pm 0.014$ GeV. In contrast, the existing measurements of the W width from the CDF collaboration at the Tevatron $p\bar{p}$ collider are much less precise:

$$\Gamma_W = 2.064 \pm 0.061(\text{stat}) \pm 0.059(\text{sys}) \text{ GeV} \tag{36}$$

from the ratio of W and Z cross sections method [33], and

$$\Gamma_W = 2.11 \pm 0.28(\text{stat}) \pm 0.16(\text{sys}) \text{ GeV} \tag{37}$$

from the shape of the lepton p_T distribution near the end-point [34]. Both measurements are evidently in good agreement with the Standard Model prediction. The weighted average of the two measurements is $\Gamma_W = 2.067 \pm 0.082$ GeV.

Concerning the impact of Γ_W on the determination of M_W, there are two points of view that one can adopt. In the context of a Standard Model fit, one can simply use the result Eq. (35) when studying the variation of the cross section with M_W near threshold. In this case, the effect on the cross section as Γ_W varies with M_W is *much* smaller than the variation with M_W directly, so that for all practical purposes Γ_W can be fixed at its nominal value of 2.078 GeV.

A less model dependent approach is to study the variation of the cross section when Γ_W is varied in its allowed experimental range, independently of M_W. Figure 8 shows the cross section near threshold for $\Gamma_W = 2.078 \pm 0.1$ GeV, as a function of $\sqrt{s}$ for fixed $M_W = 80.23$ GeV. Note that there is a stable point at $\sqrt{s} \sim 162$ GeV where the cross section is approximately independent of Γ_W. From Fig. 8 we can derive[4]

$$\Delta M \;=\; \left|\frac{d\sigma/d\Gamma}{d\sigma/dM}\right| \Delta\Gamma \;\simeq\; 0.16\, \Delta\Gamma \, , \tag{38}$$

where the derivatives are evaluated at $\sqrt{s} = 161$ GeV. Hence the uncertainty on M_W from the *current* measurement of Γ_W is ± 13 MeV. It is expected, however, that the precision of the $p\bar{p}$ collider Γ_W determination will improve significantly in the next few years [38].

A final comment concerns the use of the *running* W width $\Gamma_W(s)$ (Eq. (8)) in our calculations. It is clear from Table 2, where the cross section is computed for

[4]Note that below $\sqrt{s} \simeq 162$ GeV, *increasing* the width has the same effect on the cross section as *decreasing* the mass.

both fixed and running widths, that this *does* make a non-negligible difference in the threshold region. However the effect can be largely understood as a shift in the W mass, defined as the position of the pole in the propagator:

$$(s - M^2)^2 + (s\Gamma/M)^2 = (1 + \Gamma^2/M^2)\ (s - \overline{M}^2)^2 + (\overline{M}\Gamma)^2 \tag{39}$$

where $\overline{M} = M(1 + \Gamma^2/M^2)^{-1/2} \approx M - (\Gamma^2/2M) + \ldots \approx M - 27$ MeV. In fact, this is simply a question of the *definition* of the W mass, and is not really an additional uncertainty. The conventional procedure (used for example in the Z mass measurement at LEP) is to adopt the 'running width' definition.

3.4 Background contributions

Any additional background contributions to the cross section will reduce the sensitivity to M_W. There are two main effects: (i) the statistical error on σ_{WW} is increased by additional non-W^+W^- contributions to the event sample, and (ii) an uncertainty in the subtracted background cross section becomes an uncertainty on σ_{WW} and hence on M_W. Let us assume that the background cross section $\sigma_{\rm bkd}$ and its uncertainty $\Delta\sigma_{\rm bkd}$ are small compared to σ_{WW}. It is straightforward to show that the statistical uncertainty on M_W is increased to

$$\Delta M_{\rm stat} \longrightarrow \Delta M_{\rm stat}\ \cdot\ \sqrt{1 + \frac{\sigma_{\rm bkd}}{\epsilon \cdot \sigma_{WW}}}\ , \tag{40}$$

where ϵ is the efficiency for detecting the W^+W^- signal. The contribution to the systematic error from the uncertainty on the background cross section is given by Eq. (31), with $\Delta\sigma = \Delta\sigma_{\rm bkd}$.

A detailed quantitative assessment of all sources of background events is beyond the scope of the present work. It is however possible to give some estimates as to the likely size of the most important contributions. We can begin by classifying backgrounds into two types: *irreducible* and *reducible*. By the former we mean a four-fermion final state with the same flavour structure as a W^+W^- decay. This is dominated by non-resonant electroweak contributions to the $4f$ final state. For example, there is a non-resonant contribution to $e^+e^- \to W^+W^- \to e^+\nu d\bar{u}$ from $e^+e^- \to \gamma^*, Z^* \to e^+\nu W^- \to e^+\nu d\bar{u}$ where the W^- is radiated off an outgoing e^- produced at the γ/Z vertex.[5] Such non-resonant contributions have been studied in detail in Refs. [39] and [40]. The actual size of the additional contributions to the WW cross section depends on the particular fermion channels, the collider energy and on possible final-state cuts. A semi-analytical calculation of the background cross section [39] for a range of $4f$ final states (non-identical f, no e or ν_e) shows that in the threshold region $\sigma_{\rm bkgd}(4f)/\sigma_{WW} \ll 1\%$, and

[5] This corresponds to a 'reindeer' diagram in the language of Ref. [39].

therefore the effect on the M_W determination is negligible. It is possible that final states such as $e - \nu_e W^+$ pose more of a problem, because of the t-channel photon exchange contribution. In this case one needs a careful choice of cuts to eliminate the potentially large background cross section, see for example Ref. [40].

Reducible backgrounds have a final state which does not correspond to any $WW \to 4f$ decay channel but which in practice cannot be distinguished. By far the most important of these appears to be QCD four-jet production, $e^+e^- \to \gamma^*, Z^* \to q\bar{q}gg, q\bar{q}q\bar{q}$, which is a background to $e^+e^- \to W^+W^- \to q\bar{q}'q\bar{q}'$. Since $q\bar{q}gg$ production dominates the QCD cross section, there is practically no interference between the QCD and W^+W^- final states. Although the QCD four-jet background does not appear to cause problems in reconstructing M_W from four-jet final states well above threshold (see for example Ref. [4]), it is potentially more serious for the threshold measurement, since the W^+W^- cross section is much smaller at threshold and the QCD cross section increases with decreasing $\sqrt{s}$.

In order to gauge the size of the QCD background contribution, we have calculated[6] the cross sections for $e^+e^- \to q\bar{q}gg, q\bar{q}q\bar{q}$ in the threshold region. To define a finite-cross section we must introduce cuts which keep the massless quarks and gluons energetic and non-collinear. We do this with a simple JADE-type algorithm [42], i.e. we require that $(p_i + p_j)^2 > y_{\rm cut} s$, where $i, j = q, g$, and $y_{\rm cut}$ is a dimensionless parameter. Since this is a tree-level calculation at the parton level, it is not straightforward to relate it to the measured jet cross section. However this uncertainty can be significantly reduced by normalizing the parton-level prediction to the four-jet production rate already measured at LEP. Figure 9 shows the fraction of four-jet events measured by OPAL [43] at $\sqrt{s} = M_Z$ as a function of $y_{\rm cut}$. The curves are the theoretical predictions for two different values of the argument of the strong coupling α_s ($\mu = \sqrt{s},\ \sqrt{s}/2$) chosen to give a reasonable spread of agreement with the data. Figure 10 shows the corresponding (absolute) four-jet cross sections at $\sqrt{s} = 161$ GeV. In addition to the jet separation cut, we have required that in each event there are two jet pairs each with an invariant mass within 10 GeV of M_W. The lower dashed lines are the QCD predictions corresponding to the 'fits' in Fig. 9. The dotted line corresponds to $W^+W^- \to 4$ jets with no cuts, i.e. the total cross section multiplied by a branching ratio of 0.46 for the $q\bar{q}q\bar{q}$ final state. The solid line is the W^+W^- prediction with both types of cut included. We see that the QCD curves fall more rapidly with increasing $y_{\rm cut}$ than the W^+W^- curve, as expected from the different singularity structure of the corresponding matrix elements.

Taking the average of the dashed curves as our estimate of the QCD background, we deduce from Fig. 9 that the square root factor in Eq. (40) falls slowly from about 1.04 at $y_{\rm cut} = 0.01$ to about 1.01 at $y_{\rm cut} = 0.07$. However this improvement at large $y_{\rm cut}$ is more than offset by the overall decrease in the efficiency for detecting the signal,

[6] We use the matrix elements from Ref. [41].

which is 0.93 at $y_{\rm cut} = 0.01$ but only 0.20 at $y_{\rm cut} = 0.07$. We conclude that a small $y_{\rm cut}$ value is preferred. If we take $y_{\rm cut} = 0.01$ as representative, we obtain

$$\begin{aligned} \sigma_{WW}(4j,\ \text{no cuts}) &= 2.20\ \text{pb} \\ \sigma_{WW}(4j) &= 1.90\ \text{pb} \quad (\epsilon = 0.87) \\ \sigma_{QCD}(4j) &= 0.15 \pm 0.03\ \text{pb}\ . \end{aligned} \tag{41}$$

To estimate the overall efficiency we must include also the $q\bar{q}\ell(=e,\mu)\nu$ final state. Let us assume for simplicity that the efficiency for this channel is 87% also. Then the *total* efficiency can be estimated as[7]

$$\epsilon_{\rm all} = 0.87 \times [\ BR(W^+W^- \to q\bar{q}q\bar{q})\ +\ BR(W^+W^- \to q\bar{q}\ell\nu)\ ] = 0.65\ . \tag{42}$$

Note that a 65% efficiency leads, via Eq. (26), to an increase in the statistical error by a factor 1.24. If we assume that the background is indeed dominantly due to QCD four-jet production, then there is a further increase of 3% from the dilution factor in Eq. (40).

4 A strategy for scanning

It is anticipated that a total luminosity of $O(500)$ pb^{-1} will be obtained at LEP2. There are strong physics arguments (Higgs and other new particle searches, anomalous WWV coupling limits, ...) for running at the highest possible energies, $\sqrt{s} \sim 175 - 200$ GeV, rather than at threshold. However, given the importance of a precision M_W measurement and remembering that there *may* be a difficulty in controlling the QCD 'reconnection effects' for the $q\bar{q}q\bar{q}$ final state, it is worth giving serious consideration to using some of the available luminosity in the threshold region. Realistically, $\int \mathcal{L} = 50 - 100$ pb^{-1} could be regarded as reasonable, in which case the uncertainty on M_W obtained from the threshold cross section is predominantly statistical. One therefore has to think carefully about which collider energy (energies) are optimal. It is clear from Figs. 3 and 5 that the only sensible strategy is to run just above the nominal threshold. Notice from Fig. 4 that with this amount of luminosity there is no question of obtaining any useful information on M_W from the *shape* of the cross section alone, and so running at a single collider energy, or narrow range of energies, is sufficient. In doing so we are relying on an absolute theoretical prediction and an absolute cross-section measurement.

Of course the value of the collider energy which corresponds to maximum statistical sensitivity depends on M_W itself. *However, we already knows the W mass well enough*

[7] Note that if electrons and muons from $W \to \tau\nu$ decay are also included, this number will increase slightly.

to be able to specify this energy in advance. The sensitivity parameter K of Fig. 5 has a formal minimum at about 500 MeV above the nominal threshold of $\sqrt{s} = 2M_W$, but the variation with $\sqrt{s}$ is only slight in a region $\pm O(500)$ GeV on either side of this. Given that when LEP2 starts operation the error on M_W from the $p\bar{p}$ collider could be smaller by a factor of two than its present value of ± 180 MeV, one will know the optimal collider energy accurately enough. In addition, an initial LEP2 run at a much higher energy will allow M_W to be determined even more precisely from reconstructing the final state.

The situation would be very different if one had no *a priori* knowledge of M_W. Then it would be necessary to devise a method of locating the collider energy of maximum sensitivity without wasting luminosity. This point has been addressed in detail in Ref. [7]. It turns out that a 'data driven scanning strategy' (the BES method) can be devised. According to this one makes a sequence of measurements at different, carefully specified collider energies, continually updating the M_W determination, until one eventually arrives at the optimal energy point just above the nominal threshold. The technique has been used successfully to measure m_τ at lower energies [44].

5 Conclusions

In this paper we have investigated in detail the measurement of M_W from the W^+W^- cross section near threshold at LEP2. We have estimated the statistical and systematic uncertainties and shown that it will be the former which will dominate the error. It is therefore important to choose the collider energy carefully to maximise the sensitivity. We have shown that the optimal point is approximately 500 MeV above the nominal threshold energy, $\sqrt{s} = 2M_W$. Based on current M_W measurements, this corresponds to $\sqrt{s} \approx 161$ GeV. The actual value is not crucial within ± 500 MeV or so. Given that the existing experimental error on M_W is well within this range, there does not appear to be any need to 'scan' the threshold region to locate the most sensitive point. Our estimate for the statistical uncertainty on M_W at $\sqrt{s} = 161$ GeV is given in Eq. (26). If we assume

(i) four experiments each obtaining $\int \mathcal{L}$ of integrated luminosity,

(ii) an overall efficiency of 65%, corresponding to detecting the $q\bar{q}q\bar{q}$ and $q\bar{q}\ell(= e, \mu)\nu$ final states with an efficiency of 87%,

then our estimate is

$$\Delta M_{\rm stat} \;=\; 56 \text{ MeV} \left[\frac{\int \mathcal{L}}{100 \text{ pb}^{-1}}\right]^{-\frac{1}{2}} . \tag{43}$$

Depending on the size of the background cross section — see below — this number may increase by a few per cent.

source	ΔM_W
HO corrections	$\Delta\sigma/\sigma(\%)\ \times\ 17$ MeV
luminosity	$\Delta\mathcal{L}/\mathcal{L}(\%)\ \times\ 17$ MeV
efficiency	$\Delta\epsilon/\epsilon(\%)\ \times\ 17$ MeV
background	$\Delta\sigma\ \times\ 470$ MeV/pb
beam energy	$1.0\ \Delta E_{\rm beam}$
decay width	$0.16\ \Delta\Gamma_W$

Table 3: Summary of systematic uncertainties on M_W from a measurement of the W^+W^- cross section at $\sqrt{s} \simeq 161$ GeV.

We have also investigated various sources of systematic uncertainty, and our results are summarized in Table 3. *There does not appear to be any single dominant source.* If we assume

(i) by the time LEP2 comes into operation the theoretical cross section will be known to 1% accuracy, which is hopefully conservative,

(ii) an uncertainty of 1% on both the efficiency and the luminosity,

(iii) an uncertainty on the background cross section of $\Delta\sigma_{\rm bkd} = \pm 0.03$ pb, see Eq. (41),

(iv) a beam energy uncertainty of 15 MeV, which again is probably conservative,

(iv) either the W width is calculated in the Standard Model or will be measured with equivalent precision before LEP2,

then from Table 3 our estimate for the overall systematic uncertainty is[8]

$$\Delta M_{\rm sys} \ = \ 36 \text{ MeV} \ . \tag{44}$$

We cannot of course claim to have done a comprehensive study of *all* of the above effects, statistical or systematic, theoretical or experimental. However we have tried to use reasonable estimates to set benchmarks against which future, more complete studies can be compared. It should be clear from the previous sections where more work needs to be concentrated. Our treatment of background contributions has been superficial, to say the least. Nevertheless, our overall conclusion is that the idea of running LEP2 at the W^+W^- threshold in a dedicated attempt to measure M_W from

[8] combining the individual contributions in quadrature

the cross section is worthy of serious consideration. With an overall luminosity of order 100 pb^{-1} per experiment, the target error on M_W of ± 50 MeV could well be achievable.

A final comment concerns the impact of new physics beyond the Standard Model on this method of measuring the W mass. As already stated, we are relying on an absolute cross-section calculation, and therefore any additional new-physics contributions will distort the M_W measurement. In particular, we have shown that at $\sqrt{s} = 161$ GeV a small shift in the cross section by an amount $\Delta\sigma_{\rm new}$ is equivalent to a shift in M_W of 0.47 MeV fb$^{-1} \times \Delta\sigma_{\rm new}$. However we have seen (Fig. 1) that at threshold energies the t-channel neutrino-exchange diagram is completely dominant. The typical new-physics scenarios which have been considered would be expected to affect only the s-channel contributions; for example, anomalous γW^+W^-, ZW^+W^- couplings or new heavy boson production $e^+e^- \to Z' \to 4f$. The corresponding contributions to the cross section would therefore be suppressed by at least one additional power of β. In other words, the threshold region is probably safe from most types of new-physics contamination, at least at a level which would cause a significant shift in M_W. In any case, it is likely that a threshold energy LEP2 run would take place *after* an initial run at higher energy, in which case the presence of new physics would almost certainly have already been detected. Nevertheless, a more detailed study of new-physics contributions in the threshold region would be very desirable [45].

Acknowledgements

I am grateful to the UK PPARC for financial support in the form of a Senior Fellowship. Useful discussions with Alain Blondel, Robert Cahn, Stavros Katsanevas, Valery Khoze, Zoltan Kunszt, Alan Martin and Andrea Valassi are acknowledged. This work was supported in part by the EU Programme "Human Capital and Mobility", Network "Physics at High Energy Colliders", contract CHRX-CT93-0537 (DG 12 COMA).

Appendix

The following expressions, when substituted into Eqs. (6) and (9), give the leading-order off-shell $e^+e^- \to W^+W^-$ cross section. The results are taken from Ref. [17].

$$\begin{aligned}
a_{\gamma\gamma} &= 8\sin^4\theta_W \,\frac{1}{s^2}\, G_1(s,s_1,s_2) \\
a_{ZZ} &= \frac{1}{2}(v_e^2+a_e^2)\,\frac{1}{(s-M_Z^2)^2+M_Z^2\Gamma_Z^2(s)}\, G_1(s,s_1,s_2) \\
a_{\gamma Z} &= 4v_e\sin^2\theta_W\,\frac{1}{s}\,\frac{s-M_z^2}{(s-M_Z^2)^2+M_Z^2\Gamma_Z^2(s)}\, G_1(s,s_1,s_2) \\
a_{\nu\nu} &= G_2(s,s_1,s_2) \\
a_{\nu Z} &= -(v_e+a_e)\,\frac{s-M_z^2}{(s-M_Z^2)^2+M_Z^2\Gamma_Z^2(s)}\, G_3(s,s_1,s_2) \\
a_{\nu\gamma} &= -4\sin^2\theta_W\,\frac{1}{s}\, G_3(s,s_1,s_2)
\end{aligned} \tag{A1}$$

$$\begin{aligned}
G_1 &= \lambda^{3/2}\left[\frac{\lambda}{6}+2(ss_1+ss_2+s_1s_2)\right] \\
G_2 &= \lambda^{1/2}\left[\frac{\lambda}{6}+2(ss_1+ss_2-4s_1s_2)+4s_1s_2(s-s_1-s_2)F\right] \\
G_3 &= \lambda^{1/2}\left[\frac{\lambda}{6}(s+11s_1+11s_2)+2s(s_1^2+s_2^2+3s_1s_2)\right. \\
&\quad \left. -2(s_1^3+s_2^3)-4s_1s_2(ss_1+ss_2+s_1s_2)F\right] ,
\end{aligned} \tag{A2}$$

where $a_e = 1$, $v_e = 1-4\sin^2\theta_W$ and

$$\lambda(s,s_1,s_2) = s^2+s_1^2+s_2^2-2(ss_1+ss_2+s_1s_2) \tag{A3}$$

$$F(s,s_1,s_2) = \frac{1}{\sqrt{\lambda}}\,\ln\left(\frac{s-s_1-s_2+\sqrt{\lambda}}{s-s_1-s_2-\sqrt{\lambda}}\right) . \tag{A4}$$

References

[1] *Measurement of the W mass at LEP 200: report from the working group on mass measurement*, J. Bijnens et al., Aachen ECFA Workshop (1986).

[2] *Precision tests of electroweak physics: current status and prospects for the next two decades*, Report of the DPF Long-Range Planning Study, Working Group 1: Tests of the Electroweak Theory, convenors: F. Merritt, H. Montogomery, A. Sirlin and M. Swartz, September 1994.

[3] CDF collaboration: presented by Young-Kee Kim at the 27th International Conference on High Energy Physics (ICHEP), Glasgow, July 1994.

[4] *Report from the Working Group on LEP200 Physics*, S. Katsanevas et al., DELPHI 92-166 PHYS250 (1992).

[5] G. Gustafson, U. Pettersson and P.M. Zerwas, Phys. Lett. **B209** (1988) 90.
T. Sjöstrand and V.A. Khoze, Z. Phys. **C62** (1994) 28; Phys. Rev. Lett. **72** (1994) 28.
G. Gustafson and J. Hakkinen, Lund University preprint LU-TP-94-9 (1994).
V.A. Khoze, University of Durham preprint DTP/94/64 (1994).

[6] M.H. Austern and R.N. Cahn, preprint LBL-33780 (1994) (unpublished).

[7] He Sheng Chen and Guang Jing Zhou, Phys. Lett. **B331** (1994) 441.

[8] L3 collaboration: presentation by M. Grünewald at the 'W Mass' Working Group meeting, CERN, December 1994.

[9] DELPHI collaboration: presentation by S. Katsanevas at the 'W Mass' Working Group meeting, CERN, January 1995.

[10] ALEPH collaboration: presentation by A. Valassi at the 'W Mass' Working Group meeting, CERN, January 1995.

[11] K. Aoki, Mod. Phys. Lett. **A1** (1986) 397.

[12] K. Hagiwara, R.D. Peccei, D. Zeppenfeld and K. Hikasa, Nucl. Phys. **B282** (1987) 253.

[13] K. Hagiwara and D. Zeppenfeld, Phys. Lett. **B196** (1987) 97.

[14] Z. Hioki, Z. Phys. **C35** (1987) 113.

[15] B. Grzadkowski, Z. Hioki and J.H. Kuhn, Phys. Lett. **B205** (1988) 388.

[16] W. Beenakker and A. Denner, Int. J. Mod. Phys **A9** (1994) 4837.

[17] T. Muta, R. Najima and S. Wakaizumi, Mod. Phys. Lett. **A1** (1986) 203.

[18] A. Aeppli and D. Wyler, Phys. Lett. **B262** (1991) 125.

[19] A. Aeppli, G.J. van Oldenburgh and D. Wyler, Nucl. Phys. **B428** (1994) 126.

[20] V.S. Fadin, V.A. Khoze and A.D. Martin, Phys. Lett. **B311** (1993) 311.

[21] V.S. Fadin, V.A. Khoze and A.D. Martin, University of Durham preprint DTP/94/116 (1994).

[22] A. Sommerfeld, *Atombau und Spektrallinien*, Bd. 2, Vieweg, Braunschweig (1939); A.D. Sakharov, JETP **18** (1948) 631.

[23] D. Bardin, W. Beenakker and A. Denner, Phys. Lett. **B317** (1993) 213.

[24] V.A. Khoze, A.D. Martin and W.J. Stirling, in preparation.

[25] E.A. Kuraev and V.S. Fadin, Yad. Fiz. **41** (1985) 733.

[26] F.A. Berends, G. Burgers and W.L. van Neerven, Phys. Lett. **B177** (1986); Nucl. Phys. **B297** (1988); **B304** (1988) 921(E).

[27] M. Cacciari, A. Deandrea, G. Montagna and O. Nicrosini, Z. Phys. **C52** (1991) 421.

[28] F.A. Berends, R. Pittau and R. Kleiss, Nucl. Phys. **B426** (1994) 344.

[29] D. Bardin, A. Olchevskii, M. Bilenkii and T. Riemann, Phys. Lett. **B308** (1993) 403.

[30] J. Fleischer, F. Jegerlehner and M. Zralek, Z. Phys. **C42** (1989) 409.
F. Jegerlehner in *Radiative Corrections: Results and Perspectives*, eds. N. Dombey and F. Boudjema, NATO ASI Series, Plenum Press, New York (1990), p. 185.

[31] S. Dittmaier, M. Böhm and A. Denner, Nucl. Phys **B376** (1992) 29.

[32] S. Myers, private communication.

[33] CDF collaboration: F. Abe et al., Phys. Rev. Lett. **73** (1994) 220.

[34] CDF collaboration: F. Abe et al., Phys. Rev. Lett. **74** (1995) 341.

[35] A. Denner and T. Sack, Zeit. Phys **C46** (1990) 653.

[36] T. Sack, Fort. Phys. **41** (1993) 307.

[37] J.L. Rosner, M.P. Worah and T. Takeuchi, Phys. Rev. **D49** (1994) 1363.

[38] S. Kopp, private communication.

[39] D. Bardin, M. Bilenkii, D. Lehner, A. Olchevskii and T. Riemann, CERN preprint CERN-TH.7295/94 (1994).

[40] F.A. Berends, R. Pittau and R. Kleiss, Nucl. Phys. **B424** (1994) 308; Leiden University preprint INLO-PUB-12-94 (1994).

[41] CALKUL collaboration: D. Danckaert et al., Phys. Lett. **B114** (1982) 203.

[42] JADE collaboration: S. Bethke et al., Phys. Lett. **B213** (1988) 235.

[43] OPAL collaboration: M.Z. Akrawy et al., Phys. Lett. **B235** (1990) 389.

[44] BES collaboration: J.Z. Bai et al., Phys. Rev. Lett. **69** (1992) 3021.

[45] Z. Kunszt and W.J. Stirling, in preparation.

Figure Captions

[1] Decomposition of the Born $e^+e^- \to W^+W^-$ (on-shell) cross section into the contributions from t-channel neutrino and s-channel γ^*, Z exchange and their interferences.

[2] The cross section for $e^+e^- \to W^+W^-$ in various approximations: (i) Born (on-shell) cross section, (ii) Born (off-shell) cross section, (iii) with first-order Coulomb corrections, and (iv) with initial-state radiation. The parameter values are given in the text.

[3] The cross sections (off-shell, with Coulomb and ISR corrections) for $M_W = 80.0$ and 80.4 GeV, normalized to that for $M_W = 80.2$ GeV, as a function of the e^+e^- collider energy $\sqrt{s}$. Also shown are 'data points' with statistical errors corresponding to $\int \mathcal{L} = 100$ pb^{-1} at each energy.

[4] The cross sections (off-shell, with Coulomb and ISR corrections) for $M_W = 78.8 + 0.2n$ GeV ($0 \le n \le 4$) as a function of the e^+e^- collider energy $\sqrt{s}$ in the threshold region.

[5] The statistical sensitivity factor $K = \sqrt{\sigma}\ |d\sigma/dM|^{-1}$ as a function of the collider energy $\sqrt{s}$. The arrow indicates the position of the nominal threshold, $\sqrt{s} = 2M_W$.

[6] The multiplicative systematic sensitivity factor $J = \sigma\ |d\sigma/dM|^{-1}$ as a function of the collider energy $\sqrt{s}$. The position of the nominal threshold is indicated.

[7] The additive systematic sensitivity factor $L = |d\sigma/dM|^{-1}$ as a function of the collider energy $\sqrt{s}$. The position of the nominal threshold is indicated.

[8] Dependence of the threshold cross section on the width Γ_W.

[9] The fraction of four-jet events measured by the OPAL collaboration [43] at $\sqrt{s} = M_Z$ as a function of $y_{\rm cut}$. The curves are the theoretical predictions using the $O(\alpha_s^2)$ $q\bar{q}q\bar{q}$ and $q\bar{q}gg$ matrix elements with two different values of the argument μ of the strong coupling α_s.

[10] Four-jet cross sections from W^+W^- and QCD four-parton production at $\sqrt{s} = 161$ GeV, as a function of the jet separation parameter $y_{\rm cut}$. An additional cut requires that in each event there are two jet pairs each with an invariant mass within 10 GeV of M_W. The lower dashed lines are the QCD predictions corresponding to the curves in Fig. 9. The dotted line corresponds to $W^+W^- \to$ 4 jets with no cuts, and the solid line has both types of cut included.

This figure "fig1-1.png" is available in "png" format from:

http://arXiv.org/ps/hep-ph/9503320v1

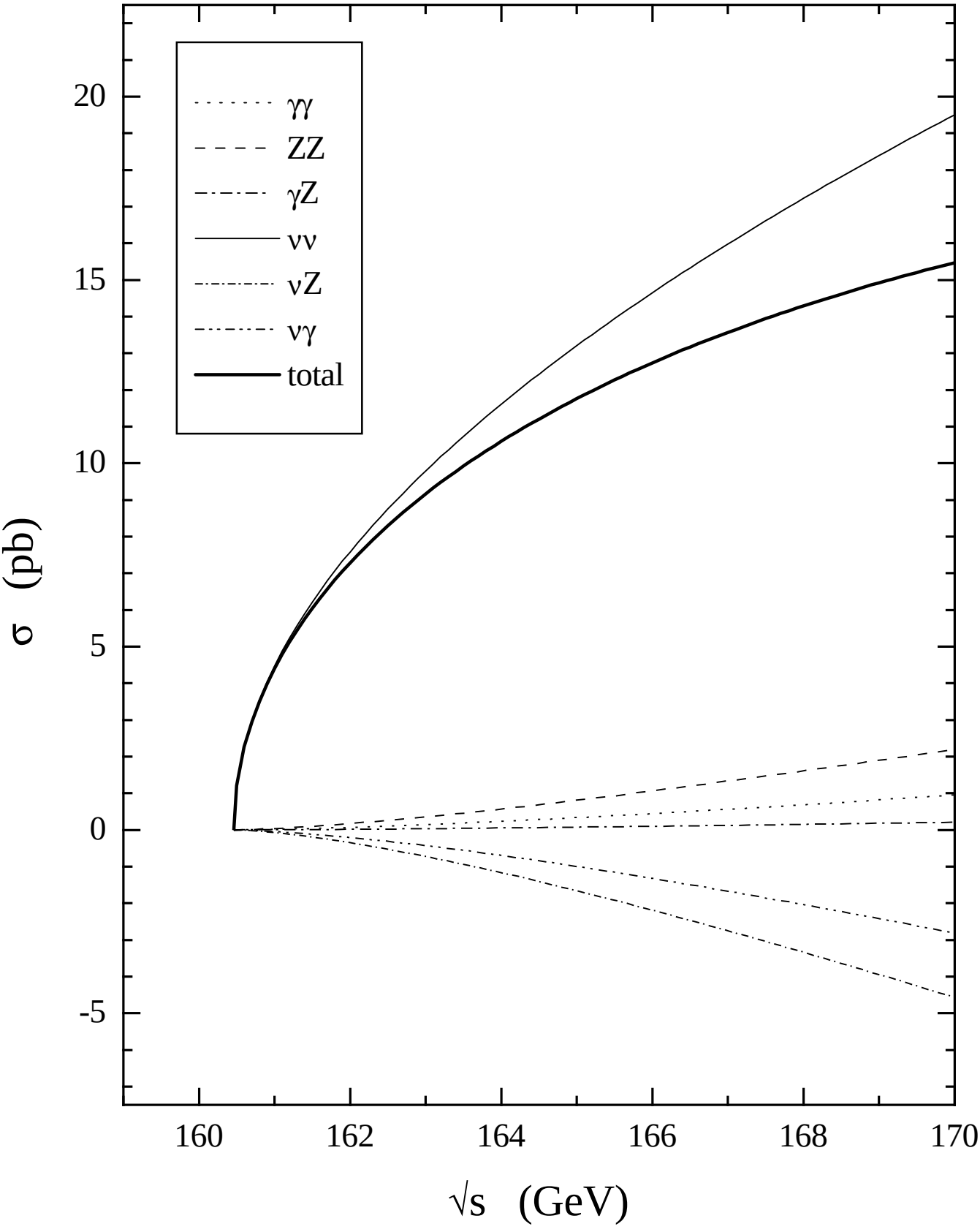
γγ
ZZ
γZ
νν
νZ
νγ
total
20
15
10
5
0
-5
σ (pb)
160
162
164
166
168
170
√s (GeV)

Fig. 1

This figure "fig2-1.png" is available in "png" format from:

http://arXiv.org/ps/hep-ph/9503320v1

This figure "fig1-2.png" is available in "png" format from:

http://arXiv.org/ps/hep-ph/9503320v1

This figure "fig2-2.png" is available in "png" format from:

http://arXiv.org/ps/hep-ph/9503320v1

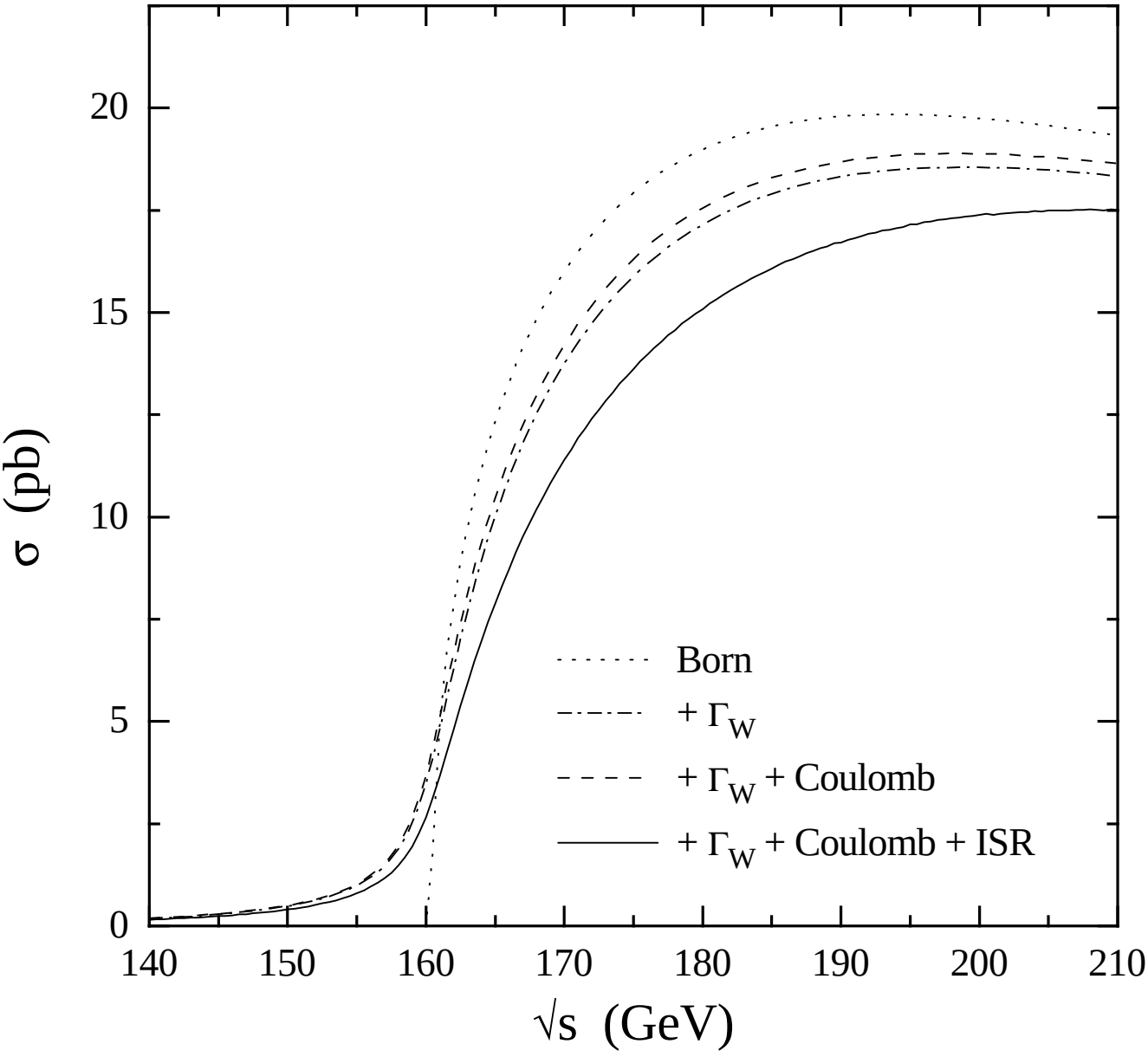
20
15
10
5
0
σ (pb)
140
150
160
170
180
190
200
210
√s (GeV)
Born
+ Γ_W
+ Γ_W + Coulomb
+ Γ_W + Coulomb + ISR

Fig. 2

This figure "fig1-3.png" is available in "png" format from:

http://arXiv.org/ps/hep-ph/9503320v1

This figure "fig2-3.png" is available in "png" format from:

http://arXiv.org/ps/hep-ph/9503320v1

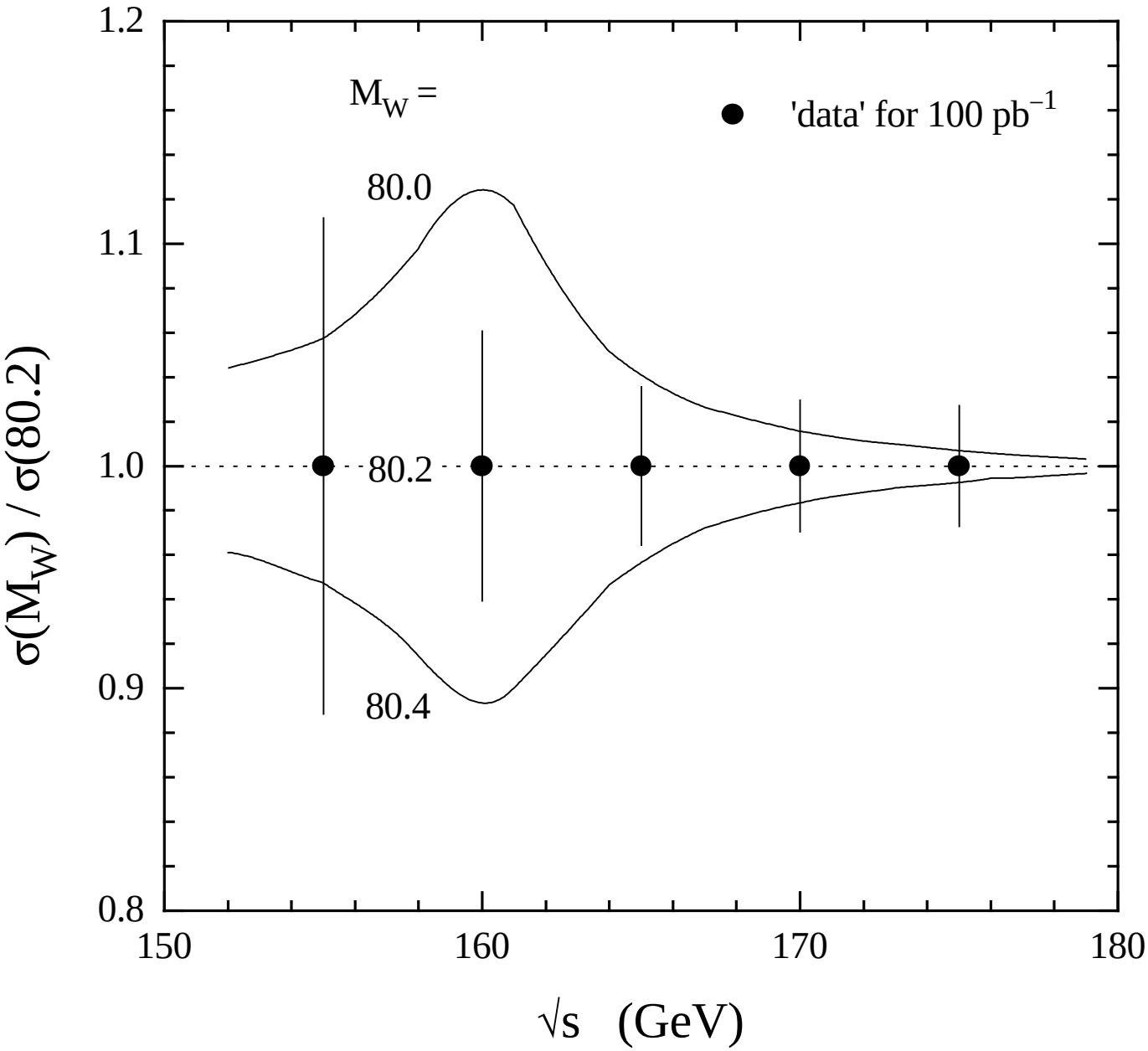
1.2
1.1
1.0
0.9
0.8
150
160
170
180
M_W =
'data' for 100 pb^{-1}
80.0
80.2
80.4
$\sigma(M_W) / \sigma(80.2)$
$\sqrt{s}$ (GeV)

Fig. 3

This figure "fig1-4.png" is available in "png" format from:

http://arXiv.org/ps/hep-ph/9503320v1

This figure "fig2-4.png" is available in "png" format from:

http://arXiv.org/ps/hep-ph/9503320v1

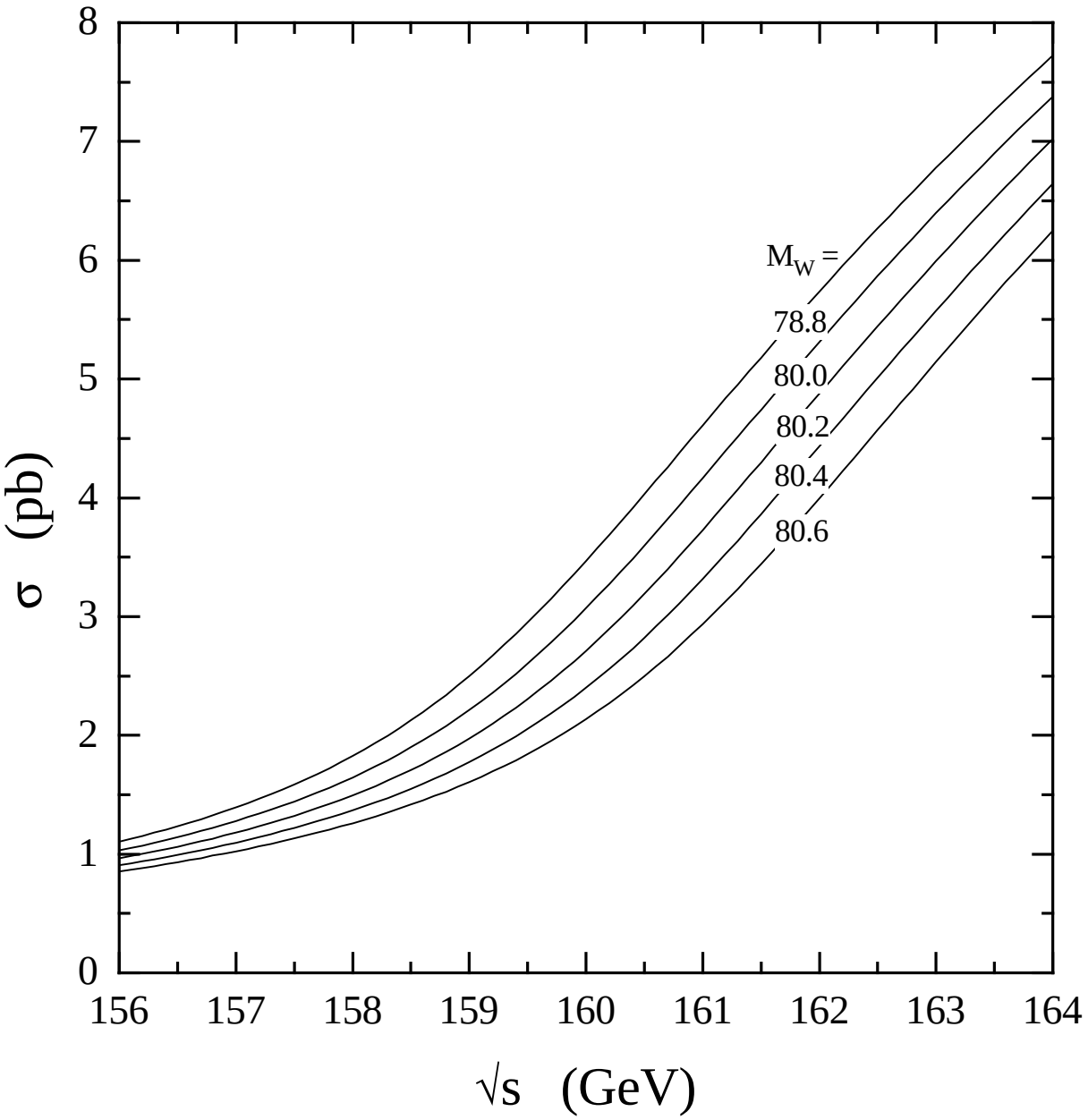
8
7
6
5
4
3
2
1
0
σ (pb)
156
157
158
159
160
161
162
163
164
√s (GeV)
M_W =
78.8
80.0
80.2
80.4
80.6

Fig. 4

This figure "fig1-5.png" is available in "png" format from:

http://arXiv.org/ps/hep-ph/9503320v1

This figure "fig2-5.png" is available in "png" format from:

http://arXiv.org/ps/hep-ph/9503320v1

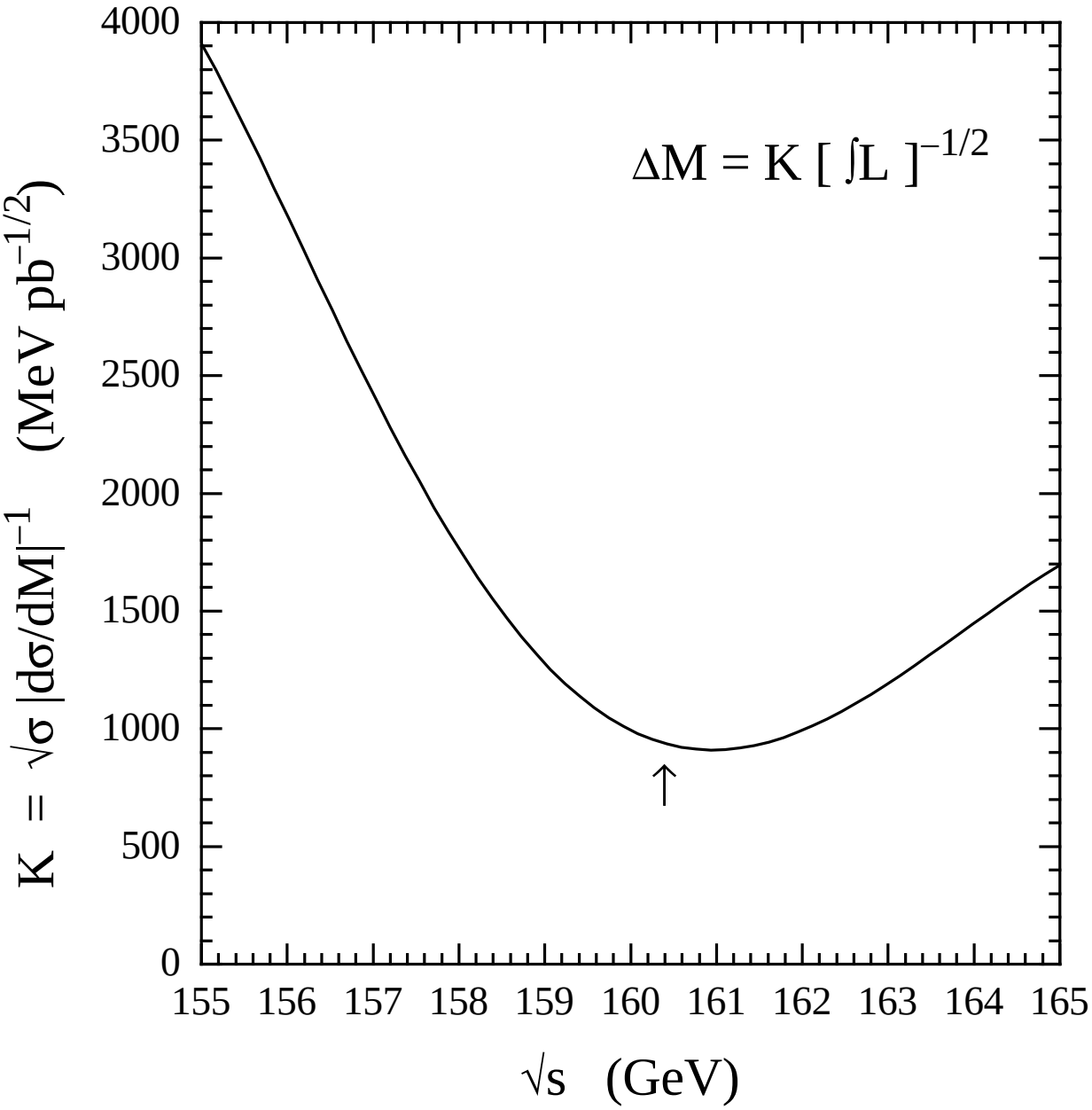
4000
3500
3000
2500
2000
1500
1000
500
0
155 156 157 158 159 160 161 162 163 164 165
$\sqrt{s}$ (GeV)
$K = \sqrt{\sigma}\,|d\sigma/dM|^{-1}$ (MeV $pb^{-1/2}$)
$\Delta M = K\,[\int L\,]^{-1/2}$

Fig. 5

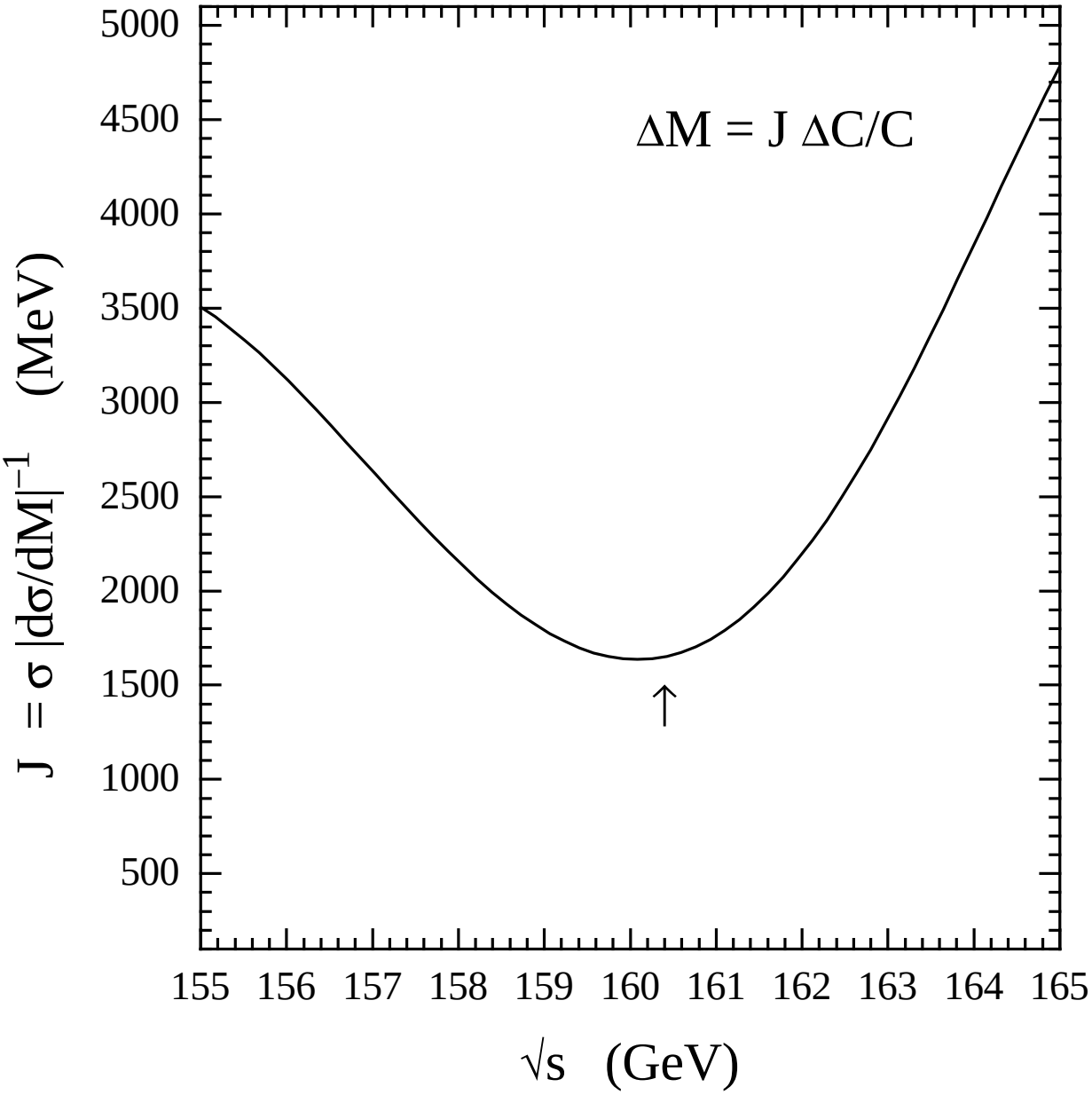
5000
4500
4000
3500
3000
2500
2000
1500
1000
500
ΔM = J ΔC/C
J = σ |dσ/dM|⁻¹ (MeV)
155 156 157 158 159 160 161 162 163 164 165
√s (GeV)

Fig. 6

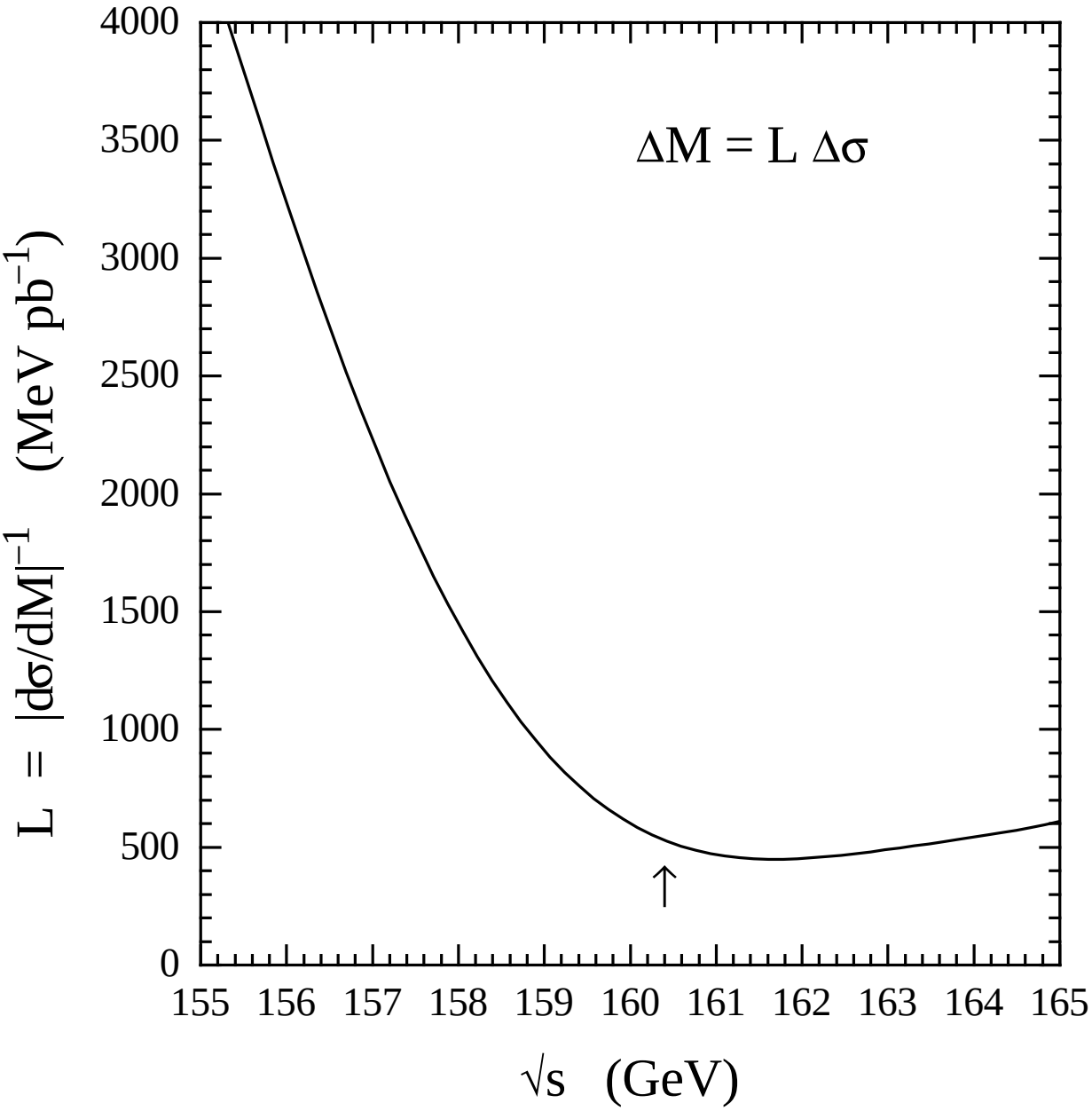
4000
3500
3000
2500
2000
1500
1000
500
0
155 156 157 158 159 160 161 162 163 164 165
ΔM = L Δσ
L = |dσ/dM|⁻¹ (MeV pb⁻¹)
√s (GeV)

Fig. 7

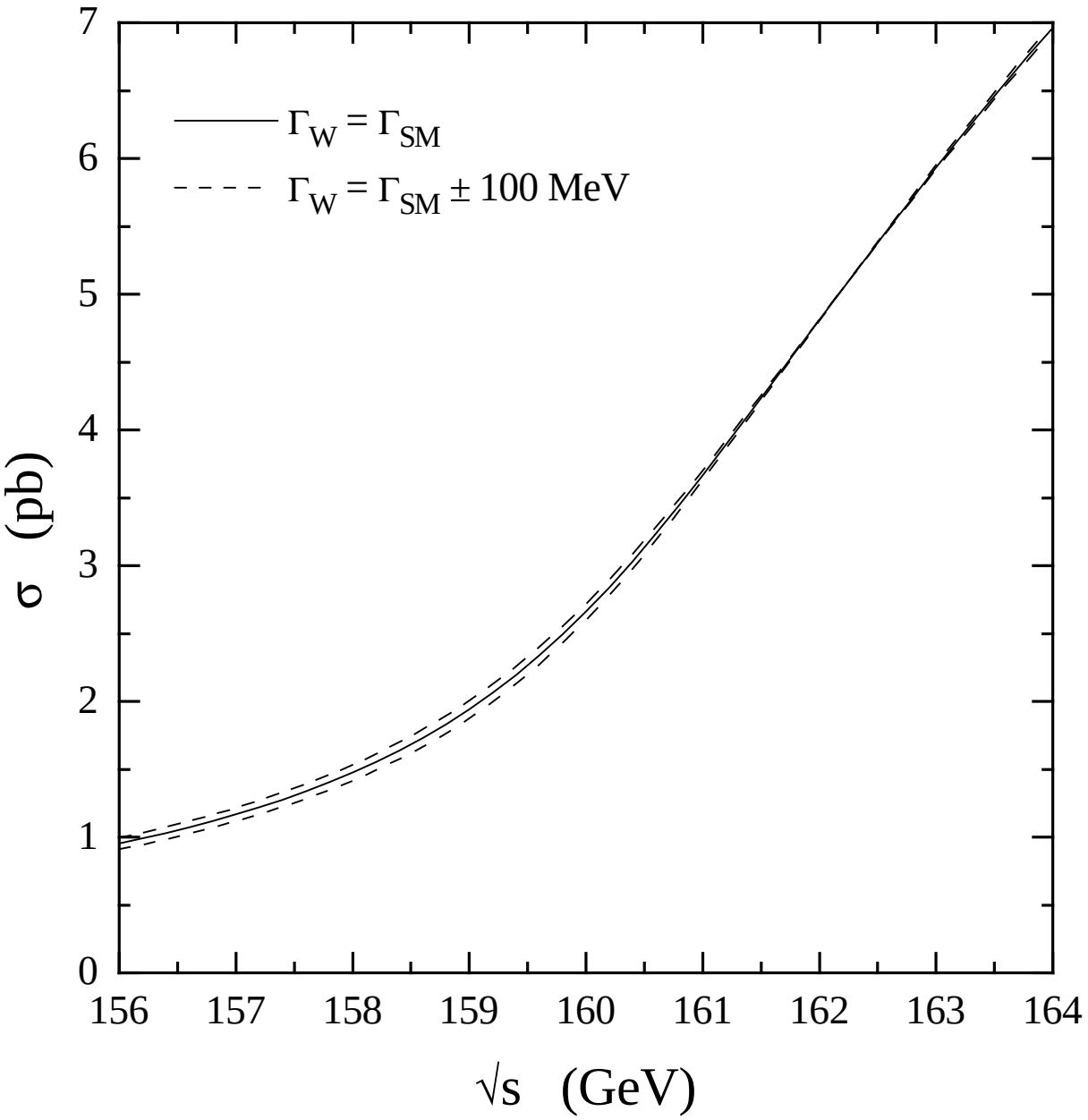
$\Gamma_W = \Gamma_{SM}$
$\Gamma_W = \Gamma_{SM} \pm 100$ MeV
σ (pb)
√s (GeV)
0
1
2
3
4
5
6
7
156
157
158
159
160
161
162
163
164

Fig. 8

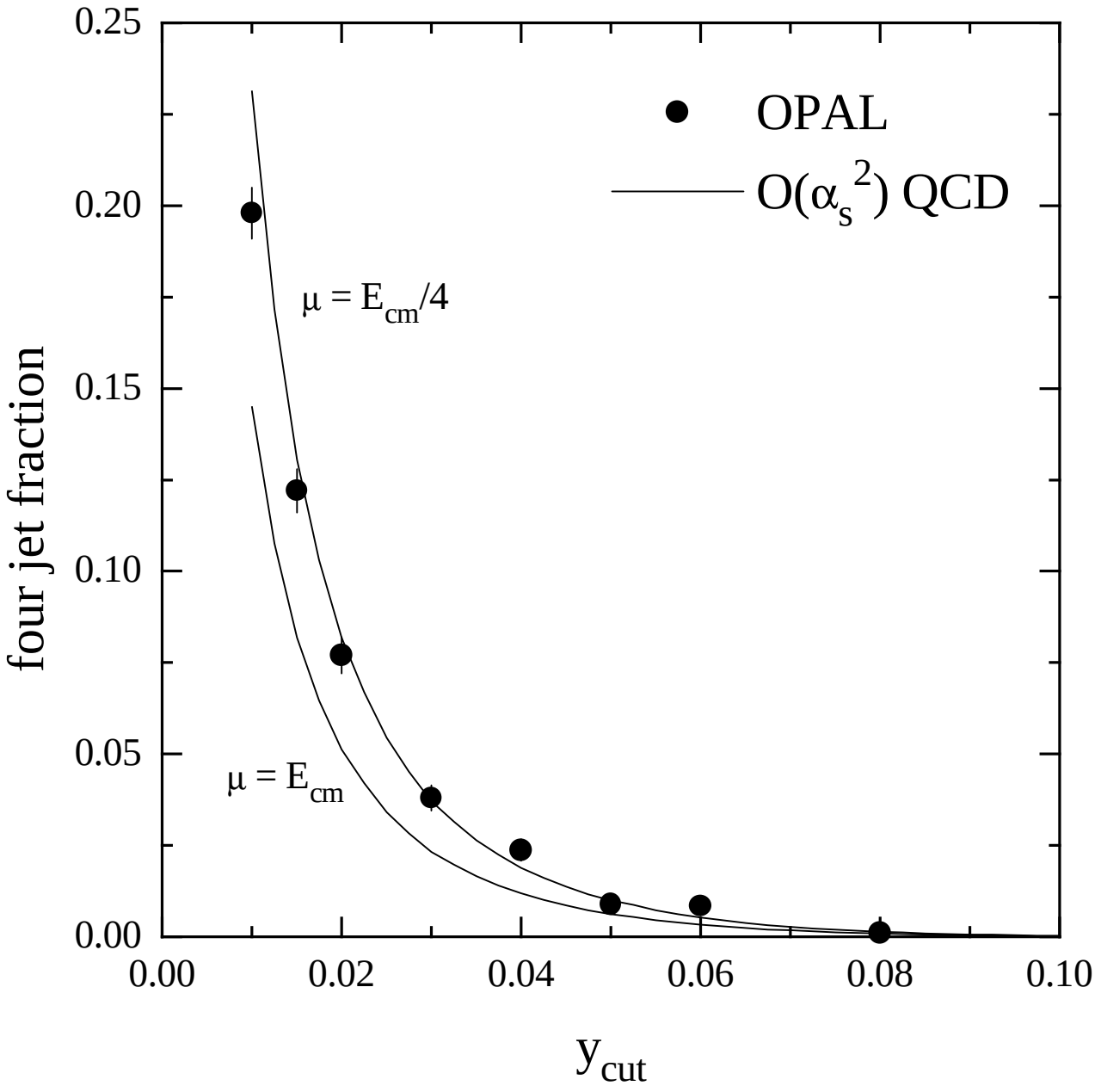
0.25
0.20
0.15
0.10
0.05
0.00
four jet fraction
OPAL
O(α_s^2) QCD
μ = E_cm/4
μ = E_cm
0.00
0.02
0.04
0.06
0.08
0.10
y_cut

Fig. 9

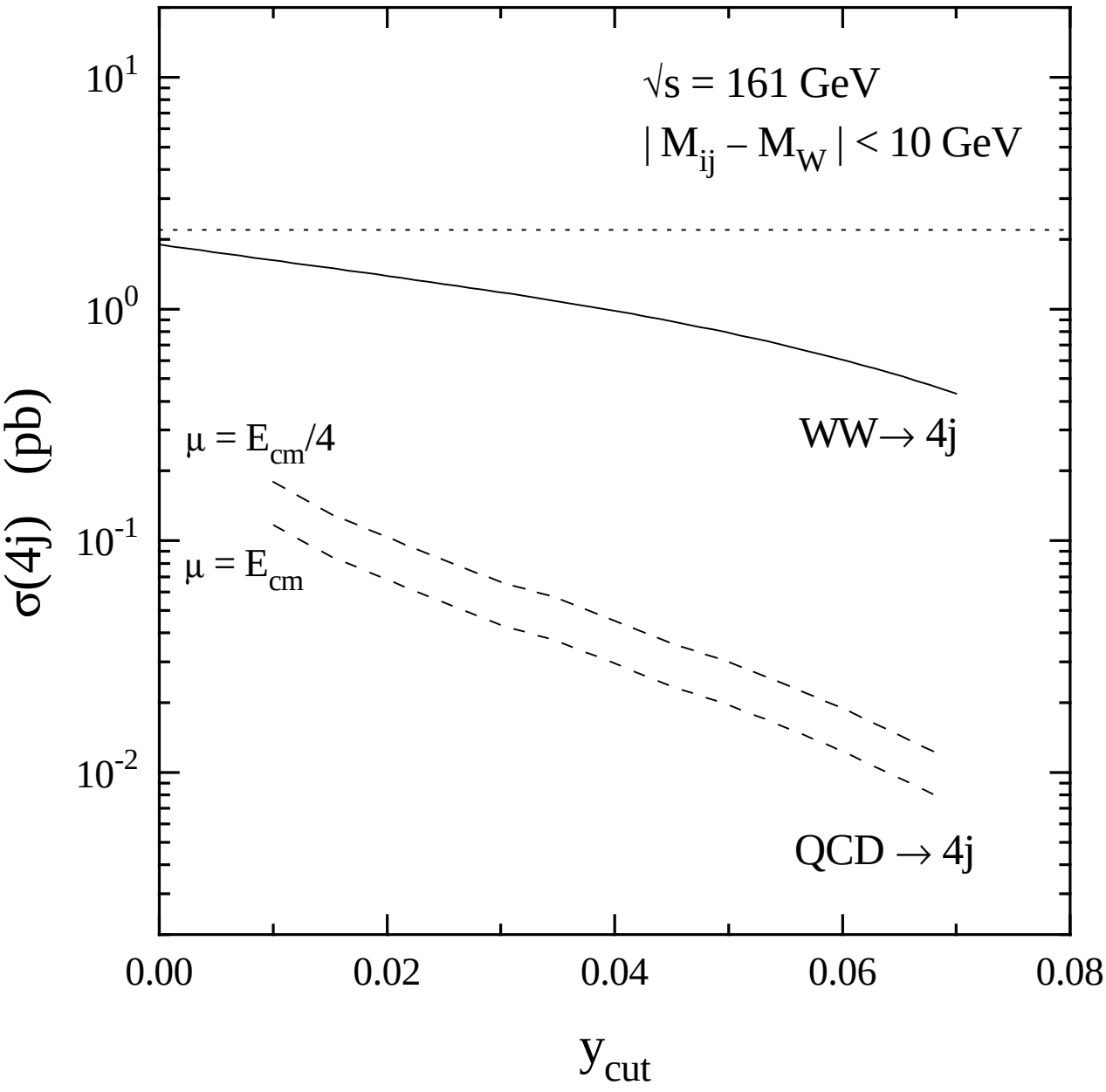
√s = 161 GeV
| M_ij – M_W | < 10 GeV
WW→ 4j
μ = E_cm/4
μ = E_cm
QCD → 4j
σ(4j) (pb)
y_cut
10^1
10^0
10^-1
10^-2
0.00
0.02
0.04
0.06
0.08

Fig. 10